# Investigation of Natural Convection Thermal Characteristics of BALI Experiment through Eulerian Computational Fluid Dynamics code and Comparison with Lagrangian code

Hyeongi Moon[1], Sohyun Park[2], Eungsoo Kim[3] and Jae-ho Jeong[1*]

[1]*Gachon University*
*1342, Seongnam-daero, Sujeong-gu, Seongnam-si, Gyeonggi-do, Republic of Korea*
[2]*Korea Atomic Energy Research Institute*
*70, Yuseong-daero 1312beon-gil, Yuseong-gu, Daejeon, Republic of Korea*
[3]*Seoul National University*
*1, Gwanak-ro, Gwanak-gu, Seoul, Republic of Korea*

*91ngk@gachon.ac.kr*

## 1. Introduction

A severe accident is an accident that exceeds Design Basis Accident, and is defined as an accident that can cause serious damage to the core and damage the integrity of the physical barriers that inhibit the outflow of radioactive materials. In-vessel corium retention through external reactor vessel cooling (IVR-ERVC) is a severe accident management (SAM) strategy that aims to arrest the downward progression of a core melt accident based on external overflow of the reactor pressure vessel. IVR-ERVC has been adopted and used in many nuclear reactors such as AP1000, APR1400, and light water reactor etc. IVR of Molten corium through the cooling of the lower head of the vessel was first introduced by Henry and Fauske, 1993 and a lot of research is still being done to this day. [1] The key to early termination of a severe accident is maintaining the integrity of the reactor vessel. However, realistic IVR experiment is impossible due to its large scale and the specificity of high Ra ($\sim 10^{16}$) and low Pr ($\sim 10^{-1}$) numbers. Accordingly, studies are being conducted to simulate the behavior of the core melt in detail via computational fluid dynamics (CFD). [2] In present study, the CFD methodology was verified by comparing the CFD results and the measured temperature near the wall and flow characteristics of the BALI experiment, which is a representative IVR-ERVC related experiment. [3]

Verification of CFD analysis methodology through comparison with BALI experimental results is almost essential before IVR-ERVC CFD analysis. [4] Among the turbulence models used for IVR-ERVC steady-state CFD analysis, there is many studies that the low-Re SST k-ω model predicts the best results. [5, 6] However, as computing power is rapidly increasing, more accurate CFD analysis is possible in much more cells compared to past studies. In this paper, the results of the steady-state CFD analysis and the unsteady CFD analysis were performed, and the comparison results with the SOPHIA, Lagrangian-based CFD code for nuclear thermal-hydraulics and safety applications, were investigated. [7, 8]

## 2. 2. MATERIALS AND METHODS

In the Severe incident, the Corium pool generates heat internally and is cooled externally by the IVR-ERVC strategy. The high Rayleigh number and low Prandtl number conditions of the corium pool show natural convection dominant thermo-hydraulic properties. The Bali program is designed to study the thermo-hydraulic properties of corium pools in either in-vessel or out-vessel situations. Fig 1 shows the schematic diagram of the BALI program. Molten corium was represented by salted water and a test section was formed with a constant thickness of 15 cm in the BALI program. Salted water is cooled under isothermal conditions of 273.15K due to ice at the bottom and top, and heated by Joule-heating of 15kW at the electrode. These dimensions give the internal Rayleigh number a value from $10^{16}$ to $10^{17}$. Since the coolant is an organic liquid that can be used between 0 and -80 degrees Celsius, an ice crust can form at the pool boundary to provide a constant temperature boundary condition. The material properties of the salted water are detailed in Table 1.

The qualitative results of the Bali experiment results are shown in Fig 2. It was observed that cold plumes appeared irregularly by top cooling, and it was

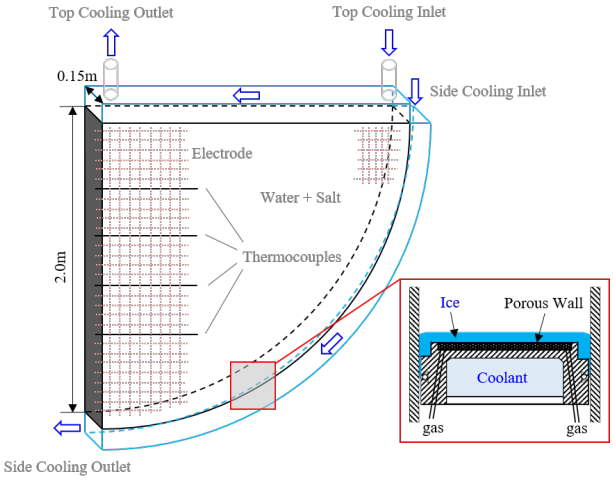


Fig 1. Schematic diagram of the BALI experiment

Table I. Salted water properties

| Property | Value | Unit |
|---|---|---|
| **Density** | 1,000 | kg / $m^3$ |
| **Dynamic viscosity** | $1.0 \times 10^{-3}$ | Pa·s |
| **Kinematic viscosity** | $1.0 \times 10^{-6}$ | $m^2$ / s |
| **Thermal expansion coefficient** | $2.7 \times 10^{-4}$ | / K |
| **Thermal conductivity** | 0.63 | W / mK |
| **Specific heat** | 4,187 | J / kgK |
| **Thermal diffusivity** | $1.505 \times 10^{-7}$ | $m^2$ / s |
| **Thermal emissivity** | 0.95 | – |

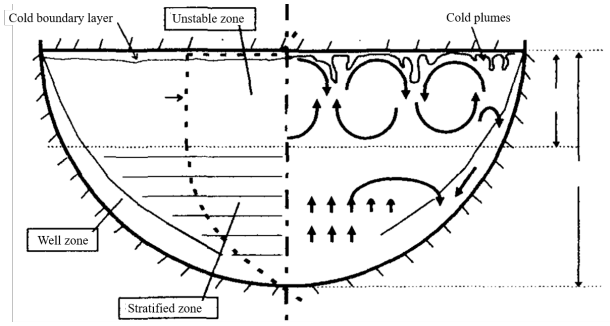


Fig 2. Qualitative results of the BALI experiment [9]

confirmed that the BALI pool can be divided into three layers: unstable, well, and stratified zone. It was analyzed whether these qualitative phenomena were simulated similarly to reality through CFD.

### 2.1. Numerical analysis methodology

Three major numerical analysis techniques, namely, direct numerical simulation (DNS) [10], large eddy simulation (LES) [11], and Reynolds averaged Navier-Stokes (RANS) simulation, can be used to analyze turbulent flow fields. To analyze the general vortex behavior precisely in a turbulent flow field containing vortices of various scales, the calculation grid size must be smaller than the minimum space scale of the vortex structure and the time interval should be less than the minimum time scale of the vortex variation. LES uses the spatially averaged Navier–Stokes equations, which directly calculate vortices greater than the grid scale and indirectly refer to the subgrid-scale model for vortices smaller than the grid scale. DNS and LES require extensive resources for their calculations, making them unfeasible in practical engineering applications. In comparison, RANS uses the time-based ensemble-averaged Navier–Stokes equations and models all of the effects caused by turbulence. Although RANS yields a lower resolution analysis than DNS or LES, it is widely used in engineering applications because it does not require high-resolution calculation grids.
In this section, governing equation of RANS and LES turbulence model are mentioned. Table 2 shows the boundary conditions of all simulations performed in this study.

Table II. Boundary condition of the simulations performed

| | |
|---|---|
| **Top Cooling Wall** | No-slip, Isothermal (273.15K) |
| **Bottom Cooling Wall** | No-slip, Isothermal (273.15K) |
| **Side Wall** | No-slip, Adiabatic |
| **Front and Back** | No-slip, Adiabatic |

#### 2.1.1. Reynolds averaged Navier-Stokes based steady simulation

There is a study result that the low-Re SST k-ω model is the most superior to the RANS analysis of natural convection due to heat transfer from the inclined wall in the closed volume, and many researchers perform IVR-ERVC analysis using the SST model. LES analysis can be performed after steady-state analysis through RANS is completed.
Turbulence models that are widely used for RANS numerical analysis in engineering include k–ε, k–ω, and SST. The k–ε turbulence model [12] precisely analyzes the turbulence behavior in free-stream regions with small pressure gradients; however, it inaccurately estimates the boundary layer separation in viscous sub-layer regions. Although the k–ω turbulence model, which was developed by Wilcox [13], accurately analyzes the separation caused by adverse pressure gradients, it is sensitive to the free-stream region. Menter [14] combined the advantages of the k–ε and k–ω models and proposed the SST turbulence model. Simulation of the wind turbine flow generally involves the use of CFD to analyze the performance of the cross-sectional airfoil of the blade, and the numerical analysis and experimental results are often in agreement [15,16]. Table 3 shows the number of cells, the turbulence model, etc. To reduce the computational resources required for analysis as much as possible, a grid was constructed using hexahedral cells.

Table III. Steady state simulation environment and settings

| | |
|---|---|
| **Package** | Star-CCM+ |
| **Solver type** | Pressure-based |
| **Turbulence model** | BSL, k-ε, SST k-ω |
| **Number of cells** | 6,252,090 |
| **Cell type** | Hexahedron |
| **Gravity model** | Boussinesq model |
| **Scheme** | High resolution |

### 2.1.2. Large eddy simulation based unsteady simulation

The governing equations for LES are obtained by filtering the time-dependent Navier-Stokes equation in a physical space. The filtering process filters out vortices smaller than the filter width or grid spacing used in the calculation.
Table 4 shows the tools and conditions used for the LES calculation. The BALI experiment, which shows the dominant flow phenomenon in the natural convection of high Rayleigh and low Prandtl number, was simulated by filtering with the Smagorinsky SGS model. To capture vibration characteristics, $\Delta t$ = 0.6s was set to ensure the resolution for vibration, and the vibration characteristics were investigated via FFT (Fast Fourier Transform) analysis.

### 2.2. Comparison of Lagrangian-based simulation and Eulerian-based solver simulation

In this paper, comparison of SPH (Smoothed Particle Hydrodynamics) based solver SOPHIA and Eulerian-based solver Star-CCM+ is performed. SPH is the most representative Lagrangian particle-based method. [17] Since SPH is mesh-free method, it is ideal to simulating the phenomena dominated by complex boundary dynamics like free surface flows or large boundary deformations.

### 2.3. Implementation of BALI experiment

To accurately calculate ω (specific dissipation) in the viscous sub-layer region using RANS simulation with the SST turbulence model, the minimum grid size must satisfy y+ < 1 in the viscous sub-layer simulation [20]. Fig 3 shows the grid system used for CFD analysis. The CFD analysis volume is in the shape of a quarter circle with a radius of 2 m, and the length in the thickness direction is 0.15 m. The vertical plane perpendicular to the ground and the front and back surfaces were set as adiabatic condition, and the isothermal boundary condition of 273.15 K was set for the side and top cooling surfaces. Gravity was simulated by adopting the boussinesq model, and the volume heating was set to 15kW, which is the same as the experimental conditions. To accurately resolve the boundary layer, the height of the first cell near the wall was set to 10-4m as shown in Fig 4. Table 5 shows the boundary conditions applied to the CFD analysis. The volumetric heat was set to 15 kW, the same as the experimental conditions.

Table IV. Unsteady simulation environment and settings

| | |
|---|---|
| **Package** | Star-CCM+ |
| **Solver type** | Pressure-based |
| **Turbulence model** | LES |
| **Number of cells** | 6,252,090 |
| **Cell type** | Hexahedron |
| **Gravity model** | Boussinesq model |
| **Advection scheme** | Central difference |
| **Time per iteration** | 0.6 [s] |
| **Total physical time** | 3600[s] |

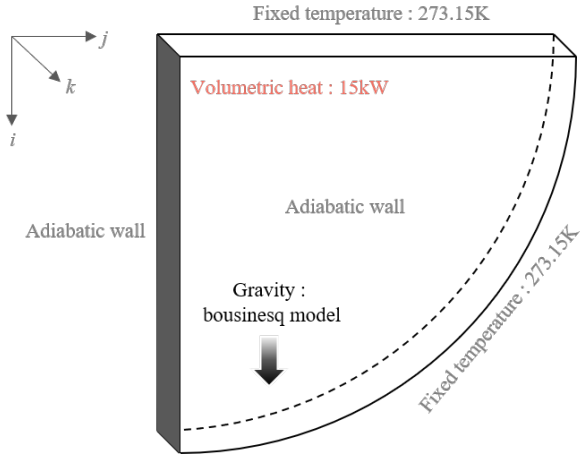


Fig 3. Grid system and boundary settings used in BALI CFD analysis

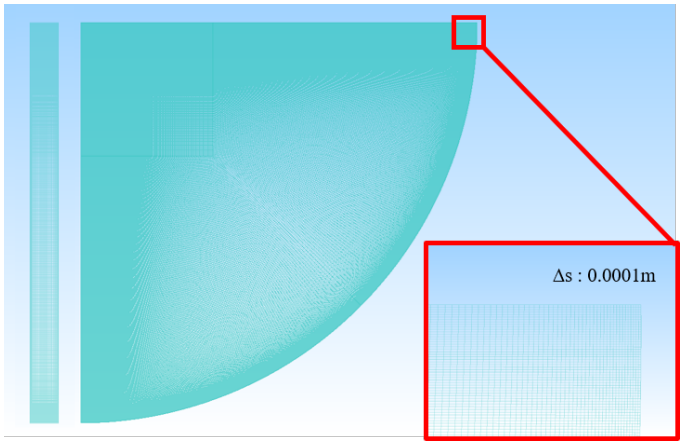


Fig 4. Boundary layer settings

Table V. Boundary conditions

| | |
|---|---|
| **Top and side boundary condition** | Isothermal, 273.15K, No-slip |
| **Vertical and glass wall boundary condition** | Adiabatic, No-slip |
| **Volumetric heat** | 15 [ kW ] |

### 3.1. CFD results analysis

In this study, steady-state CFD analysis was performed using the baseline k-ω, k-ε, and SST k-ω turbulence models. By performing unsteady CFD analysis through LES turbulence model, comparison with steady-state CFD analysis results and investigation were performed. The evaluation criteria of the convergence of all calculations were taken as the volume average temperature. The depth-temperature profile at the location of the dotted line shown in Fig 5 was compared with the temperature profile measured in the experiment.

#### 3.1.1. Reynolds averaged Navier-Stokes based simulation results

The steady state CFD results through three different turbulence model are summarized in Fig 6 and 7. Fig 6 shows the results calculated through the BSL and k-ε models were calculated depth-temperature profile with a large error compared to the measured profile through the experiment.
It was confirmed that the calculation result through the SST k-ω model showed the best agreement with the depth-temperature profile measured through the experiment with in maximum error 4°C. An environment of y+>30 for the k-ε model and y+<1 for SST is recommended. However, the mesh used for the analysis is a grid formed by considering the LES calculation, and it is formed with a larger number of cells than the grid for the RANS analysis, and y+ is calculated to be low. Therefore, it is considered that the calculation accuracy is low when the k-ε model is used and is higher when the SST k-ω model is used.

However, the SST k-ω model is advantageous for high-speed fluid analysis, and the turbulence model should not be applied to the stratified layer. In order to overcome this limitation, if LES analysis is performed, analysis with higher accuracy is possible. The calculated temperature and velocity contours for each model are shown in Fig 7.

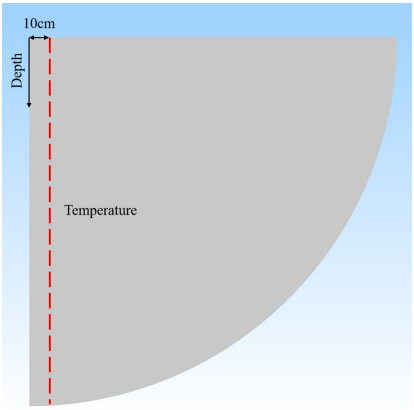


Fig 5. Temperature measurement location

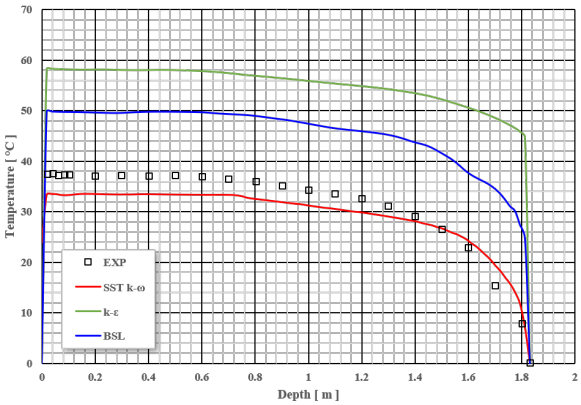


Fig 6. Depth-temperature profile of steady state calculation results

Among the calculation results, it was confirmed that the boundary between the stratified layer and the convective layer appeared more clearly in the calculation results using the BSL and SST k-ω models through the temperature contour analysis compared to the results calculated via k-ε model. The calculated temperature of the BSL model has a large error range compared to the experimental results, and the cooled water layer at the bottom observed in the BALI experiment was not observed. On the other hand, as a result of analysis through the SST k-ω model, it was confirmed that the cooled water layer at the bottom appeared through the temperature contour. Through velocity contour, it was also confirmed that the analysis results via SST k-ω has the most stable flow characteristics in stratified layer. Only the SST k-ω model simulated the 0°C layer accumulated on the bottom of the pool.

#### 3.1.2. Large eddy simulation results

As the initial condition of the LES analysis, the analysis results via SST k-$\omega$ model that best matched the experimental results were selected. Fig 8-10 show the results of the LES analysis and the SST k-$\omega$ steady-state CFD analysis.

Through the velocity contours in Fig 8, it can be confirmed that the analysis results using the LES model have distinct vortex flow characteristics and the boundary between the stratified layer and the unstable layer compared to the analysis results using the SST k-ω. In addition, it was confirmed that the thickness of the cold liquid accumulated on the bottom was thicker when analyzed using LES. In the case of BALI experiments, it is advantageous for accurate analysis that the turbulence model is not applied to the stratified layer. In the case of SST k-ω, since the turbulence model is also applied to the stratified layer, there is a

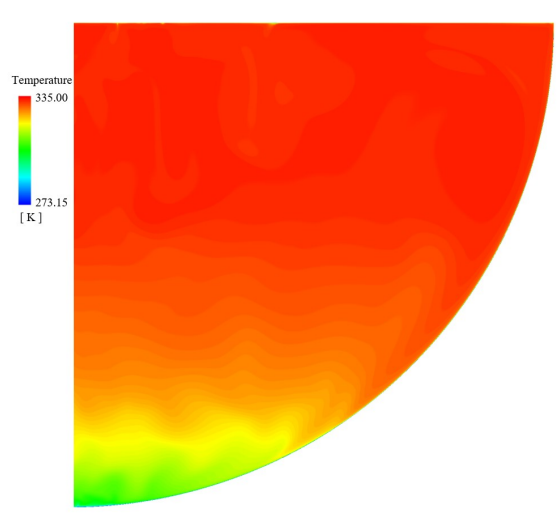


(a) Temperature – BSL

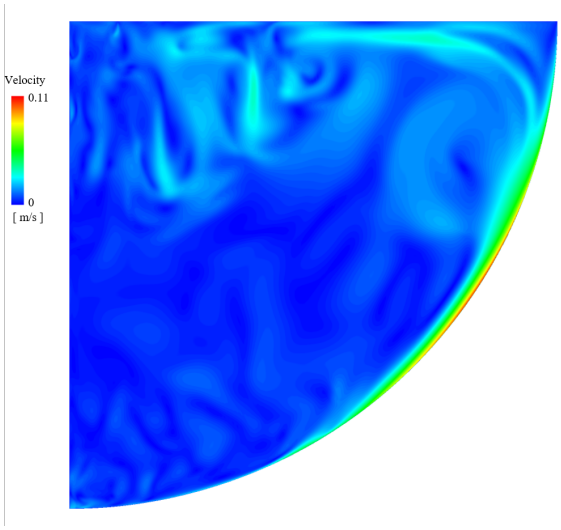


(b) Velocity – BSL

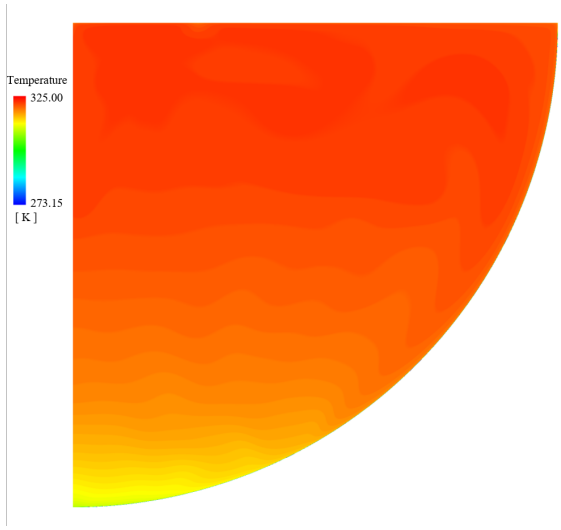


(c)Temperature – *k-ε*

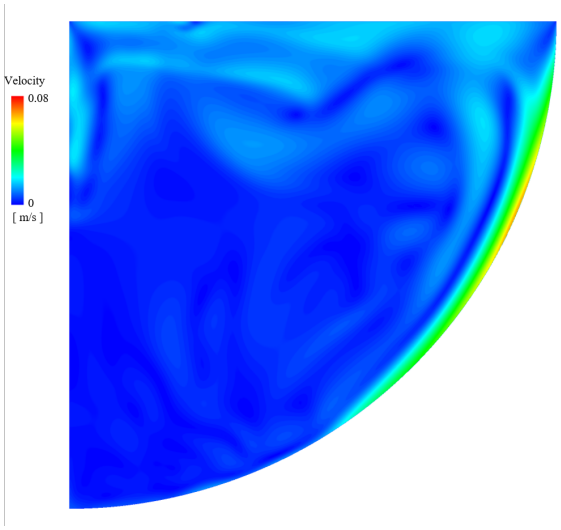


(d) Velocity – *k-ε*

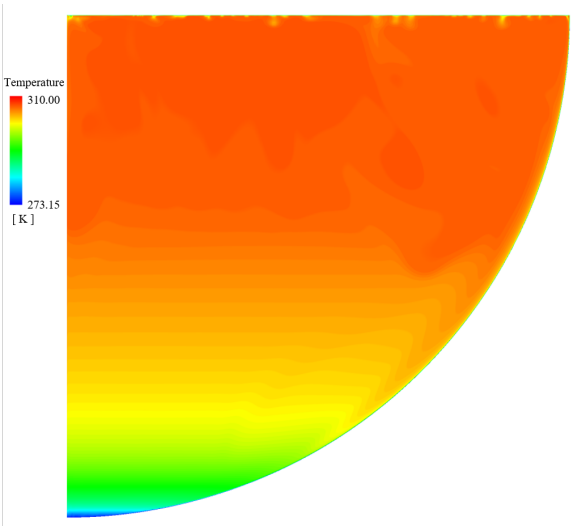


(e) Temperature – SST *k-ω*

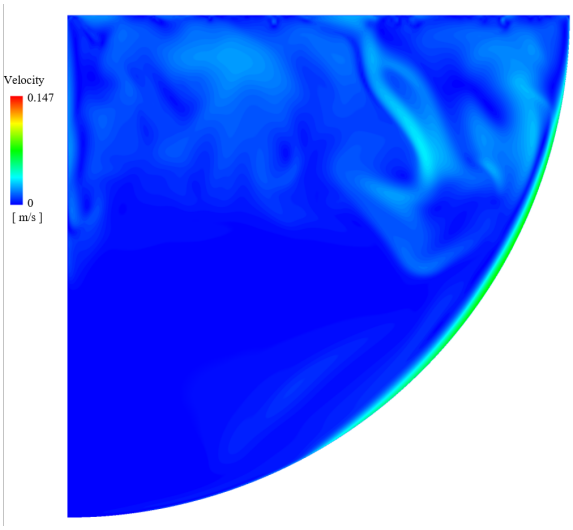


(f) Velocity – SST *k-ω*

Fig7. Steady state CFD simulation results with three different turbulence models

limitation that an accurate analysis is impossible. However, in the case of analysis through the LES model, more accurate analysis is possible because there is no such limitation. This can be confirmed through the velocity profile graph in Fig 9.

Fig 10 shows that the case of LES is easy for rough flow characteristic analysis by analyzing even smaller eddies.

Based on the results of CFD analysis through LES model, FFT analysis of pressure was performed at a total of 16 points as shown in Fig 11. Each point was positioned at a distance of 0.05 m from the wall, and P01-09 of Part 1 was formed at an interval of 10° from the contact point of the vertical wall and the top cooling wall. P10-18 of Part 2 were positioned with an interval of 0.2 m from each other, and the FFT results are shown in Fig 12 using the Barlet monitor. It was confirmed that the PSD (Pressure Spectral Density) of the points in Part 1 near the side wall was 10 to 100 times larger than in Part 2 in low frequency, which was near the top cooling wall, and had low frequency vibration characteristics. In the case of Part 1, the PSD was larger as it goes down in the direction of the stratified layer, and it was confirmed that the PSD was the largest in P09. In the case of Part 2, the PSD was smaller and did not show a clear trend compared to Part 1, but it was confirmed that the PSD of the low frequency was larger toward the side wall.

Based on the results of CFD analysis through LES model, FFT analysis of pressure was performed at a total of 16 points as shown in Fig 11. Each point was positioned at a distance of 0.05 m from the wall, and P01-09 of Part 1 was formed at an interval of 10° from the contact point of the vertical wall and the top cooling wall. P10-18 of Part 2 were positioned with an interval

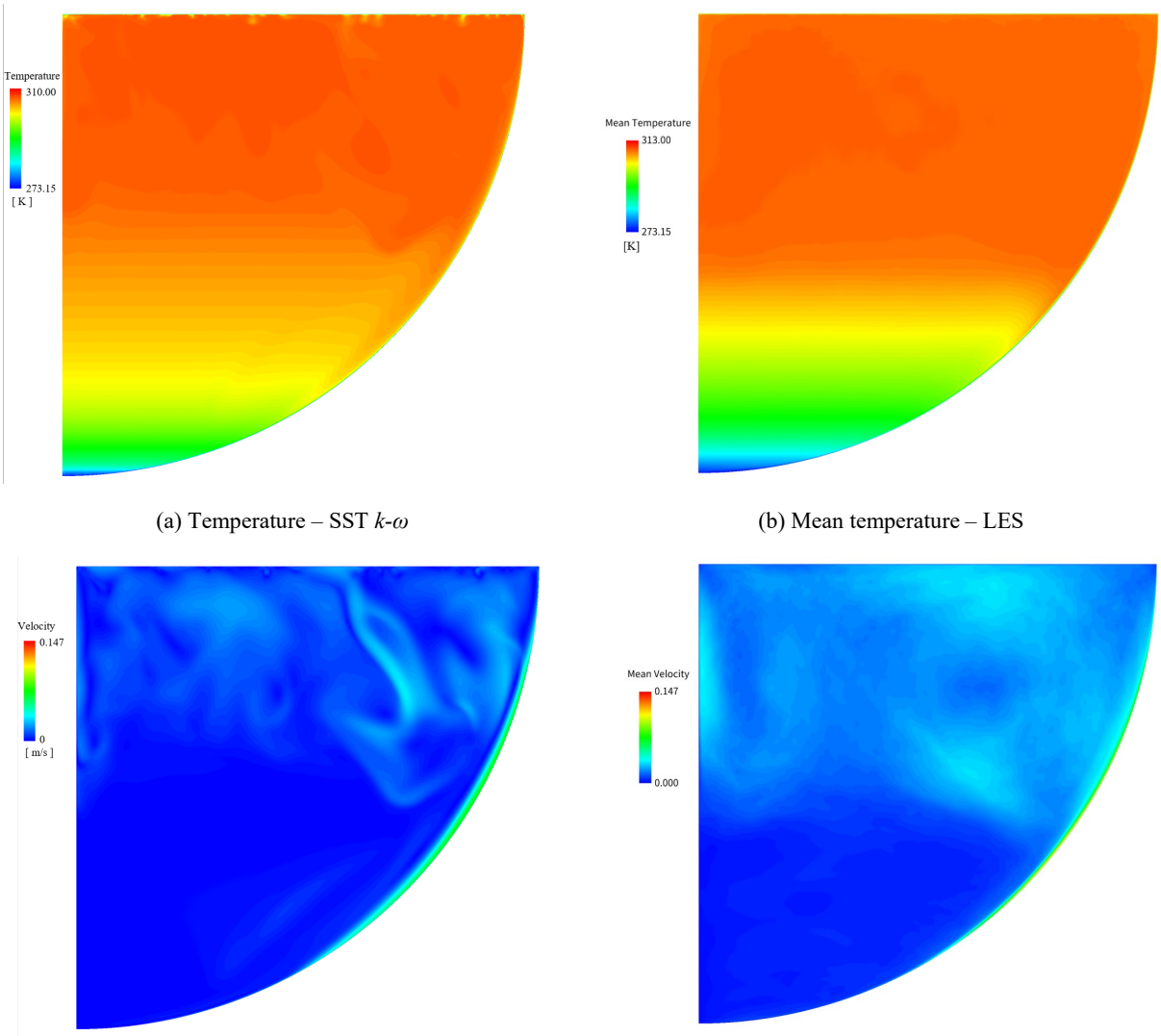


(a) Temperature – SST *k-ω*

(b) Mean temperature – LES

(c) Velocity – SST *k-ω*

(d) Mean velocity – LES

Fig 8. CFD simulation results with steady and unsteady turbulence models

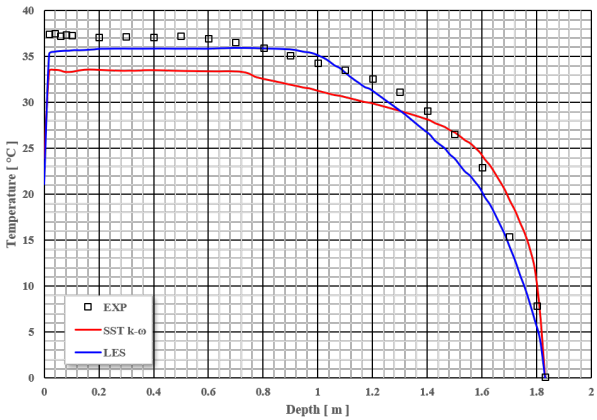


Fig 9. Depth-temperature profile of steady and unsteady calculation results

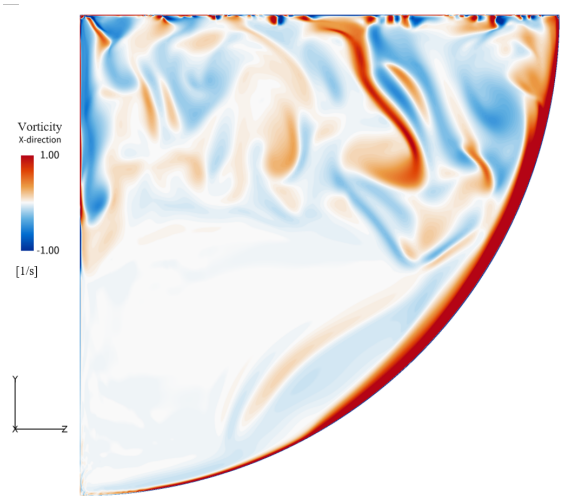


(a) Vorticity – SST *k-ω*

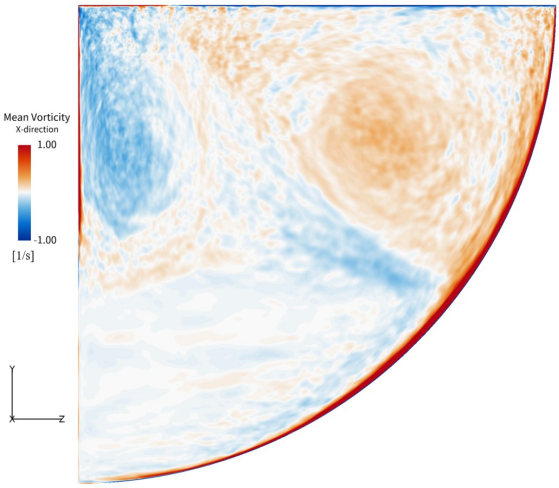


(b) Mean Vorticity – LES

Fig 10. Vorticity contour of CFD simulation results

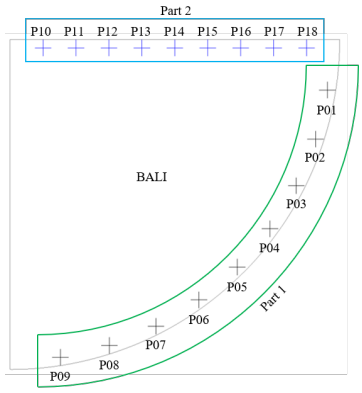


Fig 11. Position of FFT investigation points

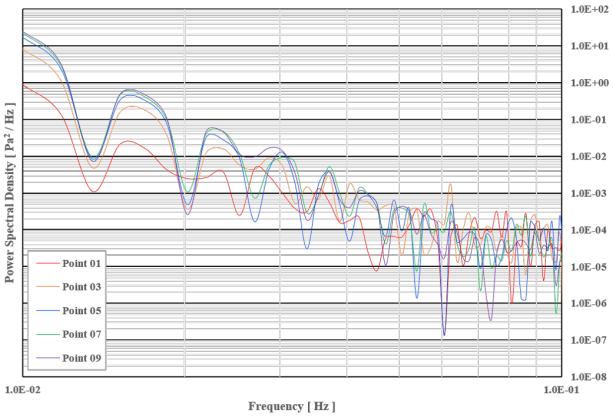


(a) Part 1

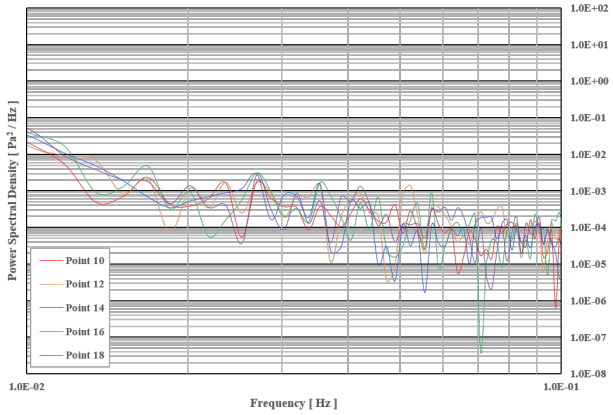


(b) Part 2

Fig 12. FFT vibration investigation result through LES analysis

of 0.2 m from each other, and the FFT results are shown in Fig 12 using the Barlet monitor. It was confirmed that the PSD (Pressure Spectral Density) of the points in Part 1 near the side wall was 10 to 100 times larger than in Part 2 in low frequency, which was near the top cooling wall, and had low frequency vibration characteristics. In the case of Part 1, the PSD was larger as it goes down in the direction of the stratified layer, and it was confirmed that the PSD was the largest in

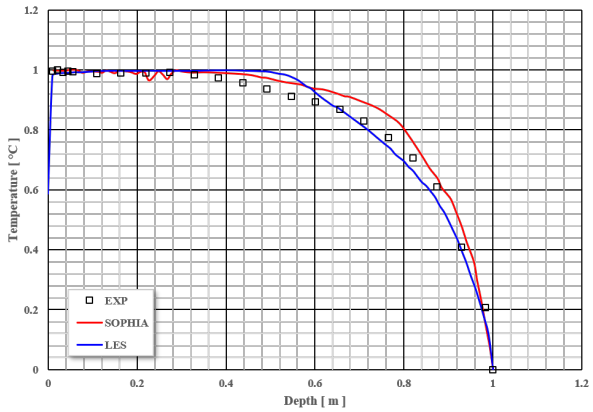


Fig 13. Depth-temperature profile of SOPHIA and LES calculation results

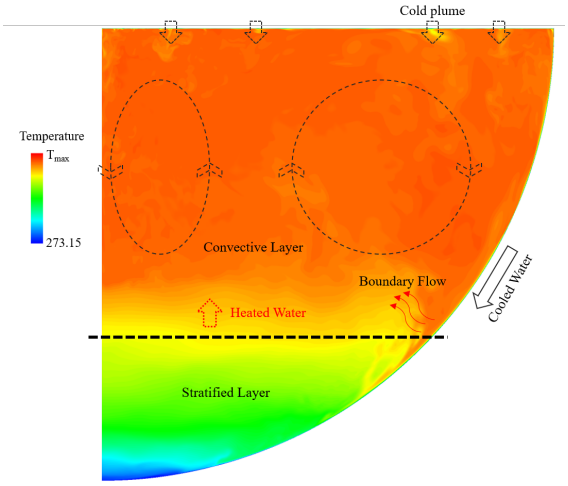


(a) LES

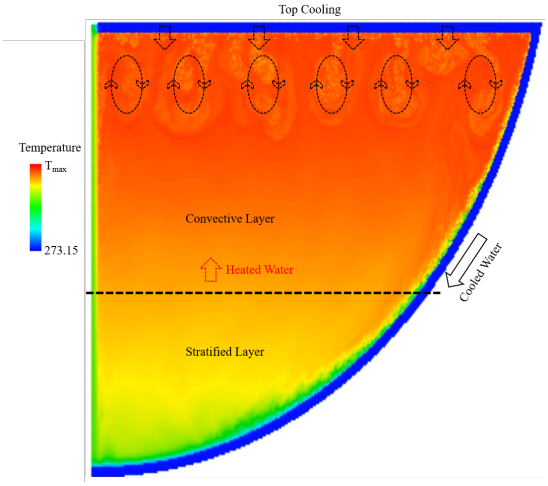


(b) SOPHIA

Fig 14. Comparison of SOHPIA and LES calculation results

P09. In the case of Part 2, the PSD was smaller and did not show a clear trend compared to Part 1, but it was confirmed that the PSD of the low frequency was larger toward the side wall.

### 3.2. Code-to-code comparison

Fig 13, 14 shows the CFD analysis results calculated through LES and SOPIHA. As a result of analyzing the depth-temperature graph in Fig 13, it was confirmed that the LES analysis results were generally better qualitatively consistent with the experimental results than the SOPHIA analysis results. However, when analyzing the graph form, the SOPHIA analysis results fit better with the depth at which the temperature begins to decrease, which means that the boundary between the convective layer and the stratified layer was calculated more accurately.

Fig 14 shows that the STAR CCM+ code simulates the convective layer wider than the SOPHIA code. This is because the SOPHIA code caught the vortex generated by the cold plume qualitatively similar to the experiment, but did not resolve the large-scale vortex flow caused by the upward flow at the boundary between the convective layer and the stratified layer. On the other hand, the STAR CCM+ code resolved the cold plume and large-scale vortex flow, and it was confirmed that it was qualitatively consistent with the experiment compared to SOPHIA. It is analyzed that the major cause of this difference is that SOPHIA is a code still under development, and calculations are performed using the k–ε model. In addition, the hot fluid also descends due to the viscosity of the cold flow descending along the bottom, and it was simulated that the hot fluid mixes into the convective layer at the boundary of each layer in LES model simulation results.

## 4. CONCLUSIONS

In this study, steady and unsteady CFD analysis for BALI experiments was performed. The steady-state CFD analysis results using three turbulence models were compared with each other, and an analysis model that best matched the experiment was derived. In addition, precise CFD analysis through LES turbulence model was performed and compared with other models. It is believed that IVR analysis can be performed through verification of the BALI CFD analysis methodology. The detailed conclusion is as follows.

- As a result of steady-state CFD analysis, among the three turbulence models k-ε, BSL, and SST k-ω, the simulation result through the SST k-ω model was the most quantitatively consistent and the maximum error was within 4°C.

- As a result of LES analysis, smaller eddies were also resolved well than RANS analysis, and the maximum error was within 2°C.

- Through FFT analysis, it was confirmed that the pressure PSD of the side wall was higher than that of the upper cooling wall, and it was confirmed that it became larger as it went down in the stratification direction.

- SOPHIA predicted the boundary line between convective and stratified layers better than LES.

- It was shown that the LES model was in quantitatively better agreement with the experimentally measured depth-temperature data compared to SOPHIA.

## 5 ACKNOWLEDGMENTS

This work was supported by Korea Institute of Energy Technology Evaluation and Planning(KETEP) grant funded by the Korea government (MOTIE) (20214000000780, Methodology Development of High-fidelity Computational Fluid Dynamics for next generation nuclear power).

## REFERENCES

[1] Henry and Fauske, 1993 External cooling of a reactor vessel under severe accident conditions R.E. Henry and H.K. Fauske Nucl. Eng. Design, 139 (1993), pp. 31-43
[2] A. Shams, D. Dovizio, K. Zwijsen, C. Le Guennic, L. Saas, R. Le Tellier, M. Peybernes, B. Bigot, E. Skrzypek, M. Skrzypek, L. Vyskocil, L. Carenini, F. Fichot, Status of computational fluid dynamics for in-vessel retention: Challenges and achievements, Annals of Nuclear Energy, Volume 135 (2020), 107004
[3] J. M. Bonnet, S. Rouge, J. M. Seiler, Large Scale Experiments for Core Melt Retention: BALI: Corium Pool Thermo hydraulics, SULTAN: Boiling under Natural Convection, OECD/CSNI/NEA Workshop on Large Molten Pool Heat Transfer, Grenoble, France (1994).
[4] Muritala Alade Amidu, Yacine Addad, Jeong Ik Lee, Dong Hoon Kam, Yong Hoon Jeong, Investigation of the pressure vessel lower head potential failure under IVR-ERVC condition during a severe accident scenario in APR1400 reactors, Nuclear Engineering and Design, Volume 376 (2021), 111107
[5] Aounallah, M. et al., 2007. Numerical investigation of turbulent natural convection in an inclined square cavity with a hot wavy wall. Int. J. Heat Mass Transf. 50, 1683–1693
[6] Jungsoo Suh, Huiun Ha, Effect of in-core instrumentation mounting location on external reactor vessel cooling, Annals of Nuclear Energy, Volume 108 (2017), Pages 89-98, ISSN 0306-4549
[7] Young Beom Jo, So-Hyun Park, Hae Yoon Choi, Hyun-Woo Jung, Yun-Jae Kim, Eung Soo Kim, SOPHIA: Development of Lagrangian-based CFD code for nuclear thermal-hydraulics and safety applications, Annals of Nuclear Energy, Volume 124 (2019), Pages 132-149, ISSN 0306-4549,
[8] OECD-NEA 1911 SOPHIA (https://www.oecd-nea.org/tools/abstract/detail/nea-1911/)
[9] Bonnet, J. M. Thermal hydraulic phenomena in corium pools; the BALI experiment. No. JAERI-CONF--99-005, 1999
[10] Orszagt, S.A. Analytical theories of turbulence. J. Fluid Mech. 1970, 41, 363–386.
[11] Smagorinsky, J. General circulation experiments with the primitive equations, i. the basic experiment. Mon. Weather. Rev. 1963, 91, 99–164.
[12] Brdina, J.E.; Huang, P.G.; Coakley, T.J. Turbulence modeling validation, testing and development. NASA Tech. Memo. 1997, 110446, 147.
[13] Wilcos, D.C. Re-assessment of the scale-determining equation for advanced turbulence models. AIAA J. 1988, 26, 1299–1310.
[14] Menter, F.R. Two-equation eddy-viscosity turbulence models for engineering applications. AIAA J. 1994, 32, 1598–1605.
[15] Andre, F.P.R.; Armando, M.A.; Herbert, M.G. An airfoil optimization technique for wind turbines. In Proceedings of the 21st Brazilian Congress of Mechanical Engineering, Natal, Brazil, 24–28 October 2011.
[16] Chen, X.M.; Agarwal, R. Optimization of flatback airfoils for wind-turbine blades using a genetic algorithm. J. Aircr. 2012, 49, 622–629.
[17] Gingold, R. A., & Monaghan, J. J. (1977), Smoothed particle hydrodynamics: theory and application to non-spherical stars. Monthly notices of the royal astronomical society, 181(3), 375-389.
[18] Molteni, D., & Colagrossi, A. A simple procedure to improve the pressure evaluation in hydrodynamic context using the SPH. Computer Physics Communications (2009), 180(6), 861-872
[19] M. Antuono, A. Colagrossi, S. Marrone, D. Molteni, Free-surface flows solved by means of SPH schemes with numerical diffusive terms, Computer Physics Communications, Volume 181, Issue 3, 2010, Pages 532-549, ISSN 0010-4655,
[20] Langtry, R.B.; Menter, F.R. Transition Modeling for General CFD Applications in Aeronautics. AIAA J. 10.2514/6., 2005-522.